

SynMVCrowd: A Large Synthetic Benchmark for Multi-view Crowd Counting and Localization

Qi Zhang¹, Daijie Chen¹, Yunfei Gong¹, Hui Huang^{1*}

¹Visual Computing Research Center, College of Computer Science and Software Engineering, Shenzhen University, Shenzhen, China.

*Corresponding author. E-mail: hhzhiyan@gmail.com;

Contributing authors: qi.zhang.opt@gmail.com;
chendaijie2022@email.szu.edu.cn; gongyunfei2021@email.szu.edu.cn;

Abstract

Existing multi-view crowd counting and localization methods are evaluated under relatively small scenes with limited crowd numbers, camera views, and frames. This makes the evaluation and comparison of existing methods impractical, as small datasets are easily overfit by these methods. To avoid these issues, 3DROM [1] proposes a data augmentation method. Instead, in this paper, we propose a large synthetic benchmark, SynMVCrowd, for more practical evaluation and comparison of multi-view crowd counting and localization tasks. The SynMVCrowd benchmark consists of 50 synthetic scenes with a large number of multi-view frames and camera views and a much larger crowd number (up to **1000**), which is more suitable for large-scene multi-view crowd vision tasks. Besides, we propose strong multi-view crowd localization and counting baselines that outperform all comparison methods on the new SynMVCrowd benchmark. Moreover, we prove that better domain transferring multi-view and single-image counting performance could be achieved with the aid of the benchmark on novel new real scenes. As a result, the proposed benchmark could advance the research for multi-view and single-image crowd counting and localization to more practical applications. The codes and datasets are here: <https://github.com/zqyq/SynMVCrowd>.

Keywords: Crowd Counting, Crowd Localization, Synthetic, Benchmark

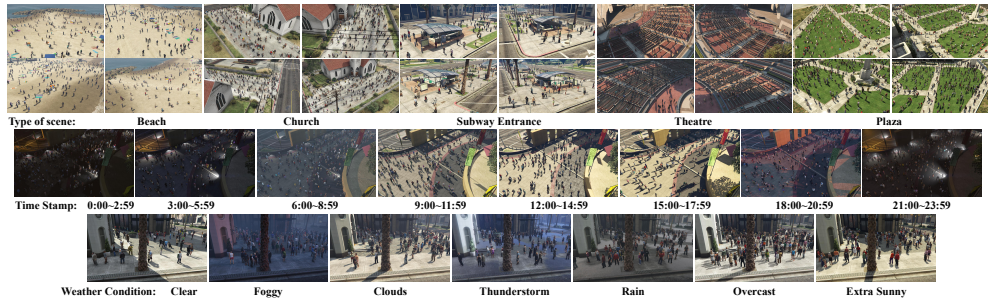


Fig. 1: The visualization of the proposed SynMVCrowd dataset: the type of scene, time stamps, and the weather condition.

1 Introduction

Crowd vision tasks include crowd counting [2], crowd detection [3], and human pose estimation [4], *etc.* To handle the severe occlusions under large scenes, multi-camera views are adopted for more challenging crowd vision tasks, such as multi-view crowd counting [5], multi-view crowd localization [6], or 3D pose estimation [7], *etc.* The existing multi-view crowd datasets [6, 8, 9] are limited in scenes, views, frames, and crowd numbers, such as the Wildtrack dataset [8] for multi-view crowd localization, which only includes 400 frames, 7 camera views, and 1 scene with about 30 people. These limitations greatly reduce the applicability of the current multi-view crowd vision methods in the real world.

However, collecting and annotating real-world multi-view image datasets with hundreds of scenes, camera views, and frames, and thousands of crowds, is too expensive. Instead, generating synthetic data becomes an alternative solution. Previous research in the area has proposed several synthetic datasets for these problems, such as MultiviewX [6]. However, MultiviewX is also a multi-view image dataset with limited camera views, scene numbers, and crowd numbers. There are also a lot of single-image-based large synthetic datasets like GCC [10], but they are not meant for multi-view settings. CVCS dataset [5] is a large synthetic dataset for multi-view counting tasks, which includes 31 scenes, with around 100 camera views and 100 frames per scene. However, the crowd number in the CVCS dataset is still too small (< 200), which is not difficult enough for multi-view settings.

To solve the mentioned problems, we propose SynMVCrowd, a large synthetic benchmark for practical multi-view-based crowd vision tasks, such as multi-view crowd counting and multi-view crowd localization. The proposed synthetic benchmark SynMVCrowd includes 50 scenes, 50 camera views, and 200 frames per scene, with around 200-1000 people in each scene. SynMVCrowd is the largest multi-view crowd dataset for various crowd vision tasks, which shall advance the multi-view crowd counting and localization from single-scene settings to cross-scene cross-view settings. With so many images of various camera perspectives, weather conditions, and light variations and scenes (see Fig. 1), SynMVCrowd could also be utilized as a large and challenging benchmark for single-image crowd counting and localization tasks. We testify the state-of-the-art multi-view crowd counting and localization methods, such as

[1, 5, 6, 11–14], on the benchmark with the cross-scene setting, which could evaluate and compare existing methods under more practical conditions. We also evaluate existing single-image crowd counting and localization methods, such as [15–17], on the proposed SynMVCrowd benchmark. Overall, the proposed SynMVCrowd benchmark could advance the research for single-image and multi-view crowd counting and localization to more practical and challenging applications. The contributions of the paper can be summarized as follows.

- As far as we know, this is the largest synthetic dataset for multi-view and single-image crowd vision tasks, which consists of a large number of crowd scenes, camera views, and frames with a large crowd number per scene.
- We evaluate and compare the existing methods on SynMVCrowd, indicating it is a challenging platform for multi-view counting and localization under cross-scene settings. We propose strong multi-view counting and localization baselines that outperform all comparisons. Besides, SynMVCrowd could also serve as a benchmark for single-image counting and localization.
- We show that better multi-view and single-image domain transferring counting performance could be achieved with SynMVCrowd. SynMVCrowd provides new directions for research on multi-view and single-image counting and localization tasks.

2 Related Work

2.1 Multi-view Crowd Counting and Localization

Multi-view crowd counting. Traditional multi-view counting methods [18–22] are typically trained on the PETS2009 dataset [9], which contains only 2 to 4 views and a few hundred frames. These methods employ foreground extraction techniques and hand-crafted features, whose performance is limited. In recent years, approaches such as [23, 24] have introduced end-to-end models that fuse cues from multiple views to enhance counting performance. [23, 24] were trained on the CityStreet dataset [23], despite its large-scale scenes, which are constrained by limited crowd density, camera numbers, and frame counts. Another notable contribution is [5], which presents a cross-view cross-scene multi-view crowd counting method and proposes a large synthetic dataset CVCS. [25] and [26, 27] tried to reduce the requirement for multi-cameras and deal with the unsynchronized and uncalibrated multi-view counting tasks, respectively. Semi-MVCC [28] proposed a multi-view ranking-based model for semi-supervised multi-view counting. CountFormer [14] adopted a transformer-based architecture for multi-view crowd counting instead of CNN-based architectures and achieved new SOTA performance. Although CVCS and CountFormer employ a synthetic dataset larger than their predecessors, it still falls short in applicability to highly congested scenes due to its restricted crowd density (with an average number of 135 in each scene).

Multi-view crowd localization. In contrast to crowd counting, multi-view crowd localization emphasizes the precision of location detection. Recent methodologies [29–31] have shifted towards projecting feature maps onto the ground plane to fuse

information from multiple RGB cameras, departing from the conventional approaches of fusing information for multi-view 2D anchors. MVDet [6] proposed a network that extracts multi-view feature maps and projects them onto the ground plane, then fuses them on the ground plane to obtain the final crowd location prediction. MVDeTr [12] incorporated attention modules to ensure optimal weight assignment to each perspective during information fusion. Building upon MVDet, SHOT [11] employs a soft-selection module for fusing cues from projection planes of different planes. 3DROM [1] dealt with the overfitting issue through a 3D cylinder data augmentation technique. SVCW [13] proposed a large scene multi-view crowd localization model by introducing extra single-view ground-plane supervision via view contribution weighting in the fusion process. MVOT [32] proposed a novel point-supervision-based optimal transport for the multi-view crowd localization task, achieving much better performance than the Gaussian density map MSE loss. TrackTacular [33] proposed to utilize a 3D projection to achieve more precise multi-view fusion features. CaMuViD [34] introduced a forward-backward projection technique that enables calibration-free multi-view crowd localization.

Overall, many of these methods are trained and tested on small-scale scene datasets with sparse crowds in local areas, which hinders their ability to generalize to novel scenes in real-world scenarios. Therefore, a large multi-view crowd dataset with larger scenes, higher crowd densities, increased scene numbers and camera numbers, and variable camera layouts, is in demand.

2.2 Multi-view Crowd Datasets

[8, 9, 23, 35] are single-scene multi-view crowd datasets captured in the real world. **PETS2009** [9], **DukeMTMC** [35] and **Wildtrack** [8] contain relatively fewer frames and crowd numbers (< 40), covering a small scene size (see Table 2). **CityStreet** [23] is an urban traffic intersection dataset containing 500 frames with 3 camera views and a larger crowd number (70-150) in the scene. In comparison to previous datasets, CityStreet significantly improves the coverage of scenes within the camera’s perspective, but it is still too small for more complicated scenarios. *To reduce the data collecting and labeling cost, synthetic scene datasets are also adopted.* **MultiviewX** [6] covers a 16×25 meters area, with 6 fixed camera views, only 400 multi-view frames, and 40 people in the scene on average. In addition, **CVCS** [5] is a large dataset with 31 diverse scenes and 31,000 multi-view frames in total, averaging 60 to 120 camera views and 90-180 people per scene. Notably, CVCS significantly surpasses MultiviewX in crowd density, scene size, and annotated image count. We conclude that current multi-view datasets still contain a small number of crowds in the scene (< 200), which is not suitable for more practical applications. Thus, a more challenging multi-view dataset with more crowds is in demand.

2.3 Single Image Counting and Localization

Early single-image methods [36–44] design multi-scale networks to address the scale variation issues. [45–51] and CSRNet [15] used the context information to alleviate the non-uniform crowd distribution. Besides, [52–54] have proposed different loss

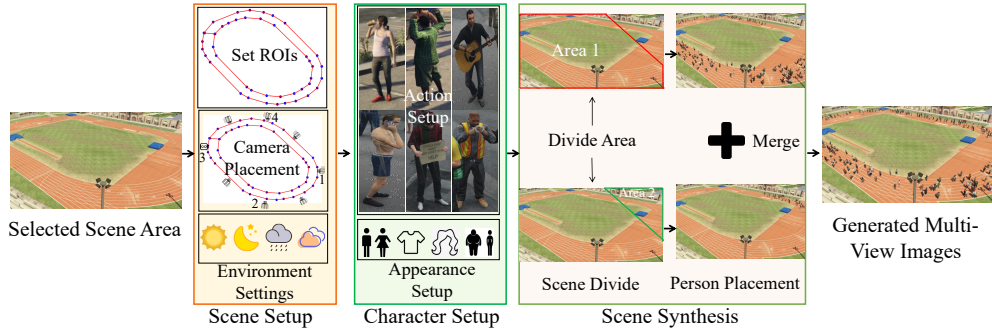


Fig. 2: The whole process of the multi-view crowd image generation, including scene setup, character setup, and the scene synthesis.

functions to improve the model’s attention to high-density crowd areas for better counting performance. P2PNet [17] and DM-Count [16] utilize point supervision without applying Gaussian kernels to dot maps. GramFormer [55] improves crowd counting by using graph-modulated transformers to diversify attention and weight features by node importance. FreeLunch [56] boosts multi-modal crowd counting by adding cross-modal alignment and regional density supervision with no extra data, parameters, or inference cost. Recently, some researchers have turned to semi-supervised and weakly supervised methods [57–60] to make the model perform better in the absence of data.

Existing single-image datasets include ShanghaiTech [2], UCSD [61], UCF-CC-50 [62], UCF-QNRF [63], MALL [64], WorldExpo’10 [65], NWPU [66], and JHCrowd [67]. In addition to real-scene datasets, [10] proposed a large synthetic single-image crowd-counting dataset called GCC. However, GCC is a single-image dataset and is not suitable for multi-view crowd vision tasks. In contrast, SynMVCrowd aims to serve as a challenging platform for both multi-view and single-image crowd counting and localization tasks.

3 Benchmark Creation and Analysis

We first introduce how to generate the proposed benchmark SynMVCrowd, and then compare its statistics with existing multi-view and single-image crowd datasets.

3.1 SynMVCrowd Benchmark Creation

We extend the GTA-V synthetic platform of GCC [10] for generating multiple view frames, the full process is illustrated in Fig. 2, consisting of three steps: scene setup, character setup, and scene synthesis. The scene setup step first defines the Region of Interest (ROI) for placing the people and excludes some invalid regions where people are unlikely to appear, and sets up the camera locations to cover the whole scene as much as possible, and the environment settings, eg, weather and timestamps. In the character setup step, we define the action and appearance of the character in the scene on the GTA-V platform. For scene synthesis, we first divide the whole scene into several areas, then we place the crowd in each area, and record the crowds with

the camera views. Finally, we merge different crowd areas to form a large crowd and generate multi-view images of the crowd.

3.1.1 Scene Setup

In the scene setup step, we first select a possible area as the scene background, and set up ROIs to place the crowd. Then, we place the cameras around the scene ROIs to cover the whole scene as much as possible. At last, we also need to set up the environmental conditions, such as weather, light, or timestamps.

ROIs setup. In each scene, we manually design a Region of Interest (ROI) area for placing the crowd. First, we carefully design the scene shape of each scene to make the scenes contain as many people as possible. At the same time, to prevent unreasonable situations where people are standing on the top of buildings or obstacles, we need to define a suitable area of the scene for the crowd placement. Specifically, when constructing each scene, we mark a number of boundary points in the scene so that they are connected to form a specific area to limit the area generated by the character models, as seen in ‘Set ROIs’ of Fig. 2 Top Left.

Camera placement. Based on the scene ROIs, we set up the camera locations around the ROIs. First, we use four camera views to observe the scene in the four directions of east, south, west, and north, as the cameras 1-4 in Fig. 2 Top Left. The angle difference between each adjacent camera view pair is approximately 90 degrees. Based on the first four cameras’ orientations and locations, we built a camera sequence to circle around the scene. In the sequence, each camera faces the center of the scene area, forming a circular zone around the scene. The offset angle between each adjacent camera view pair is approximately 10 degrees, and the field of view of the camera is 40 degrees. Overall, in the camera sequence, we create 46 different new camera perspectives, each with similar heights and pitch angles, as well as different locations and rotation angles. Including the first four camera views, there are a total of 50 camera views.

Environment settings. We construct 50 scenes that frequently occur in real life, such as parks, walking streets, beaches, shopping centers, churches, and so on. Besides, we include various weather conditions (clear, cloudy, rainy, thunderstorm, foggy, overcast, and extra sunny) and light variations (0-24h) in the scene to increase the diversity of the background environments. Fig. 1 illustrates the exemplars under various kinds of weather at different times. The two pie charts in Fig. 3 respectively show the proportional distribution of weather conditions and timestamps for the proposed dataset:

- **Weather:** The GTA-V game engine provides 7 different types of weather conditions, including Clear, Extra Sunny, Overcast, Clouds, Rain, Foggy, and Thunder, and 0-24 hours timestamps. We use hook scripts to control all these weather and time conditions as the background environment. Specifically, we firstly set ‘Clear’ as the most common weather conditions, which account for 50% images in the dataset. Then, using different weather conditions as the control group, we employ a randomization function to assign all weather conditions to the remaining 50% of the dataset according to a predefined weighting ratio. Based on synthetic crowd

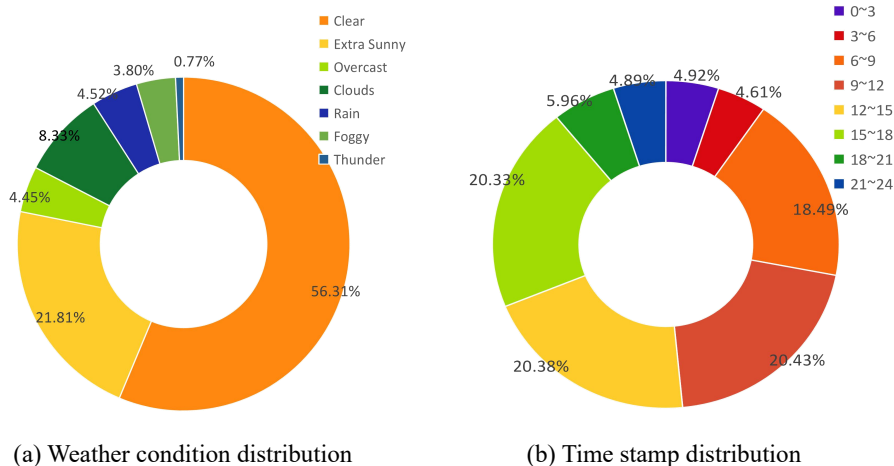


Fig. 3: The two pie charts respectively illustrate the distribution of time stamps and weather conditions in SynMVCrowd. On the right side, each label denotes a time of 24 hours.

image rendering results, the weighting distribution is defined as 2:1:1:1:1 for the following conditions: extra sunny, clear, overcast, cloudy, rain, and foggy. And after removing examples with incorrect label information, finally, as shown in Fig. 3 (a), the distribution probabilities of all weather are: Clear 56.31%, Extra Sunny 21.81%, Overcast 4.45%, Clouds 8.33%, Rain 4.52%, Foggy 3.80%, and Thunder 0.77%. Due to the rendering effect of the crowd under the thunder weather, we only adopt this weather in some special scenarios, accounting for only 0.77% of all data.

- **Timestamp:** Similarly, the time conditions also use the same strategy to control. Specifically, we divide all time conditions into five main parts: Morning (from 6 a.m. to 9 a.m.), Noon (from 9 a.m. to 12 p.m.), Afternoon (from 12 p.m. to 3 p.m.), Sunset (from 3 p.m. to 6 p.m.), and Evening (from 6 p.m. to 6 a.m.). Different parts share the same weight ratio (defined as 1:1:1:1). In addition, Evening time is longer than other time conditions, so we additionally divide time periods, including night (from 6 p.m. to 9 p.m.), nightfall (from 9 p.m. to 12 p.m.), midnight (from 12 p.m. to 3 a.m.), and early morning (from 3 a.m. to 6 a.m.). Among Evening time, different periods also share the same weighting distribution. Finally, after filtering data with incorrect labels, as shown in Fig. 3 (b), the distribution of timestamps in each part is approximately 20%. From 6 p.m. to 6 a.m., the average for each timestamp is approximately 5%.

3.1.2 Character Setup

In GTA-V, it provides 265 character models, each character designed to exhibit distinct physical characteristics that enhance the authenticity of the in-game world. For instance, each model has different physical characteristics, such as skin color, hairstyle, clothing, body shape, gender, *etc.* Additionally, the characters have varied physical



Fig. 4: The action catalog of SynMVCrowd, consisting of various human poses in daily life.

builds: ranging from ‘thin’ and ‘sturdy’ to ‘obesity’. Variations in height and body proportions further ensure that no two characters feel identical. To enable precise tracking and distinguish these characters, each person has a specific ID for mapping their coordinates in the world coordinate system and their locations in each camera-view image. Besides, in order to make the stationary character models more realistic, we give each person a random action. These actions are carefully designed to avoid disrupting the fixed positions of the characters. Unlike dynamic actions (e.g., running, jumping) that involve movement, these actions are subtle and localized. As shown in Fig. 4, characters adjust the movements of their upper body, such as smoking, drinking, music, and so on. What’s more, the distribution of crowd numbers is based on their space capacity to increase the number of people present in each scenario (see Fig. 5).

3.1.3 Scene Synthesis

Scene divide and person placement. After the scene setup and character setup are successful, we will place people in the ROI area. GTA-V has a maximum number limit (256) of people in a scene. To synthesize more congested crowd scenes, we generate the scene step by step. Specifically, as shown in Fig. 2, we first divide the scene into two areas: Area 1 and Area 2. Next, we will place part of the character models in Area 1 and record this area with 50 cameras immediately. Next, we delete all the character models in that area and place other character models in Area 2, and record the camera

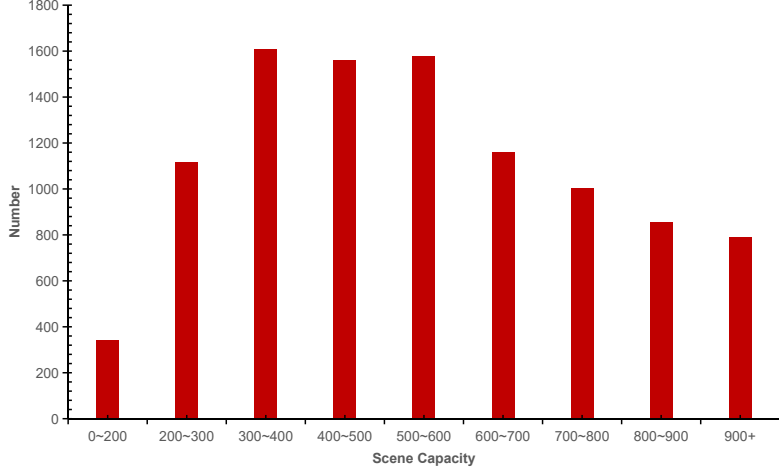


Fig. 5: The frame numbers of crowd count distributions of SynMVCrowd.

Table 1: The statistical comparison of the proposed SynMVCrowd and six existing multi-view crowd datasets.

Dataset	Type	Scenes	Size	Cameras	Frames	Average Resolution	Counting Statistics			
							Total	Min	Avg	Max
PETS2009 [9]	Real	1	-	3	1,899	576×768	-	20	-	40
DukeMTMC [35]	Real	1	-	4	989	1080×1920	-	10	-	30
Wildtrack [8]	Real	1	12×36	7	400	1080×1920	-	-	20	-
MultiviewX [6]	Syn	1	16×25	6	400	1080×1920	-	-	40	-
CityStreet [23]	Real	1	58×72	3	500	1520×2704	64K	70	128	150
CVCS [5]	Syn	31	90×80	60-120	3,100	1080×1920	418.5K	90	135	180
SynMVCrowd	Syn	50	100×120	50	10,000	1080×1920	5.3M	151	530	1,000

views again. If the area contains more character models, the divided area will continue to be split, and the area of each region will further shrink.

Scene merge. Eventually, we integrate all the area images into one scene and produce a set of multi-view frames for the scene. When merging, the area image is a scene image with partial crowd information, and the background image is a scene image that fully covers the crowd regions. The difference between the two images represents the pixel values of the crowd. By recording the pixel differences between all areas and the background image and adding them to the same background image, we can obtain the synthetic scene image. And during the process of picture recording, we adjusted the time flow rate of the game to ensure that the background of the pictures in different areas did not change.

3.2 SynMVCrowd Analysis and Comparison

We generate a series of scenes that frequently occur in real life to enrich the data distribution of the dataset. As shown in Figure 6, SynMVCrowd contains 15 different scene types and consists of 50 different urban scenes. Among them, the number of scene



Fig. 6: The scene examples of SynMVCrowd. The orange box contains a perspective from the training set. The green and blue boxes contain a perspective from the validation and test sets.

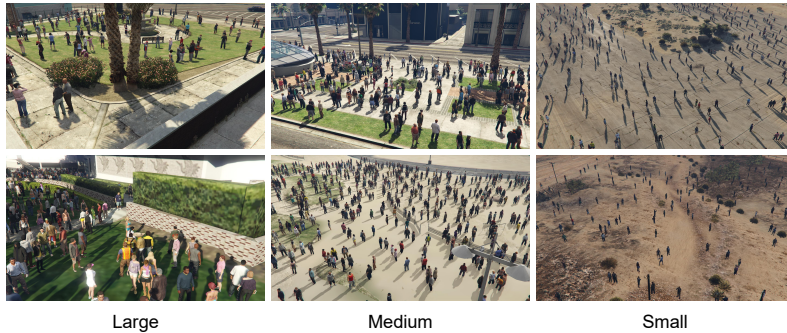


Fig. 7: The dataset samples of scale variations.

types, such as curbside, park, and beach, is larger than other scene types, because these scenarios are widespread in our daily lives. According to different scene types, we divide the training set, test set, and validation set in a ratio of 3:1:1. The training set includes 30 scenes and 14 scene types in total. There are 10 scenes in the validation set and the test set, respectively, where the test set contains more scenario types than the validation set. Each scene contains 200 multi-view frames, comprising 50 camera views and 10 thousand different images. In total, SynMVCrowd consists of 500,000 images. And the training set contains 300k images, the test set and validation set contain 100k images (scene number * camera views * frame number). We show the visualization result of the divided dataset in Figure 6.

What's more, we carefully considered the scale variation in the real world, since we contain scenes of variable sizes, and the crowds in the scenes vary with scale, as in Figure 7. We also generate accurate crowd semantic segmentation images and crowd

Table 2: The statistic comparison of the proposed SynMVCrowd and nine existing single-image crowd datasets.

Dataset	Type	Year	Average	Number	Counting Statistics			
			Resolution	of Images	Total	Min	Avg	Max
USCD [61]	Real	2008	158×238	2,000	50K	11	25	46
Mall [64]	Real	2012	240×320	2,000	62K	13	31	53
UCF_CC_50 [62]	Real	2013	2101×2888	50	64K	94	1,280	4,543
WorldExpo'10 [65]	Real	2015	576×720	3,980	200K	1	50	253
ShanghaiTech Part A [2]	Real	2016	589×868	482	242K	33	501	3,139
ShanghaiTech Part B [2]	Real	2016	768×1024	716	88K	9	27	57
GCC [10]	Syn	2019	1080×1920	15,212	7.6M	0	501	3,995
UCF_QNRF [63]	Real	2019	2013×2902	1,535	1.3M	49	815	12,865
NWPU-Crowd [66]	Real	2020	2191×3209	5,109	2.1M	0	418	20,033
SynMVCrowd	Syn	2024	1080×1920	500,000	5.3M	47	530	1,000

coordinates in the image and the world coordinate system, with a special ID for each person. Furthermore, we record all auxiliary information in each scene in detail, which includes camera parameters, weather conditions, time, scene size *etc.* For each scene, we set up 50 camera views to record the crowd information of the scene and repeat 200 times to capture different crowd distributions under various weather conditions in the scene. Thus, each scene contains 200 multi-view frames, comprising 50 camera views. In total, the whole dataset consists of 500,000 images, with a resolution of 1920×1080 pixels, each image contains crowds ranging from 200 to 1000, with an average of more than 500 people.

Comparison with multi-view datasets. In order to further demonstrate the superiority of our proposed dataset, we compare the proposed SynMVCrowd dataset with other multi-view crowd datasets in Table 1. PETS2009 [9], DukeMTMC [35], Wildtrack [8] and CityStreet [23] are all single-scene real-world datasets. Due to the difficulty of collecting realistic data, the distribution of crowd numbers and background environments in these four realistic datasets is simple. PETS2009 [9] and DukeMTMC [68] contain a small number of crowd (<40). In Wildtrack [8] and MultiviewX [6], the scale of the scene is relatively small, only within 12×36 meters area. In CityStreet [23], though the scene size and crowd numbers have been enlarged, a scene with only 3 camera views is relatively small. CVCS [5] is a large synthetic dataset that can provide data on the distribution of different populations in multiple scenarios under different background environments, but each scene contains a sparse crowd with small crowd numbers. In contrast, the proposed SynMVCrowd contains more scenes, more crowds, higher densities, and more frames, which are more suitable for comprehensively validating crowd vision tasks.

Comparison with single-image datasets. Compared with the existing single-image crowd-counting datasets, SynMVCrowd is the largest one from the perspective of the image level. Table 2 summarizes the statistics of the single-image crowd-counting datasets. Before 2016, many datasets had the disadvantage of low resolution, such as USCD [61], Mall [64], and WorldExpo'10 [65], whose average resolution was less than 600×800, and the number of images was less than 4,000. On the other hand,

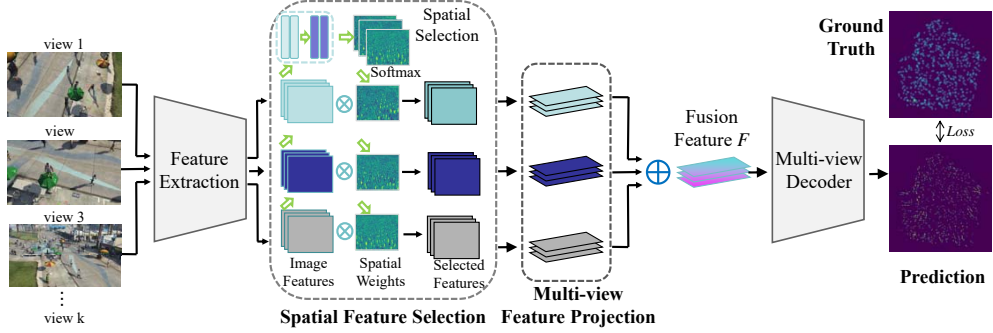


Fig. 8: The pipeline of multi-view localization and counting baseline model: single-image feature extraction, spatial feature selection, multi-view feature projection and fusion, and multi-view decoding with MSE or Optimal Transport (OT) loss.

UCF_CC_50 [62], ShanghaiTech Part A and B [2] with less than 1,000 images will easily cause over-fitting problems. In more recent datasets, GCC [10], UCF_QNRF [63], and NWPU-dataset [66] have a wider range of people and higher resolution. Compared with previous works, GCC is a synthetic dataset with the largest number of images, around 15,000 images. However, compared to previous single-image datasets, SynMVCrowd can provide 5.3 million images for training, with various scene and perspective variations, weather, and lighting changes. Overall, the proposed SynMVCrowd benchmark is a challenging platform for existing multi-view and single-image crowd counting and localization methods, which shall advance the research of crowd counting and localization to more practical applications.

4 SynMVCrowd Benchmark Evaluation

In this section, we evaluate and compare the SOTA multi-view and single-image crowd counting and localization methods on the proposed SynMVCrowd benchmark. Besides, we propose a strong multi-view crowd counting and localization baseline, outperforming all existing methods.

4.1 Multi-view Crowd Localization

4.1.1 Baseline Method

We propose a strong multi-view localization baseline, whose pipeline is shown in Fig. 8, which consists of 4 modules: single-view feature extraction, spatial feature selection, multi-view feature projection and fusion, and multi-view decoding. The single-view feature extraction module uses feature extraction backbone nets (eg, ResNet-18, VGG19, or Transformer) for extracting the features of input images. The effect of the spatial feature selection module is to select effective features in a spatial-attention fashion. Specifically, we input each single-view feature into the spatial feature selection module, and it first estimates the spatial attention map of each view, which is then normalized with a softmax layer across all views. The spatial attention map is multiplied by the input view features to select useful features.

Then, the filtered single-view features are projected to the scene ground plane via a projection layer based on the spatial transformation network [69], where Translation between 3D locations (x, y, z) and 2D image pixel coordinates (u, v) is done via

$$s \begin{pmatrix} u \\ v \\ 1 \end{pmatrix} = P \begin{pmatrix} x \\ y \\ z \\ 1 \end{pmatrix} = A [R|t] \begin{pmatrix} x \\ y \\ z \\ 1 \end{pmatrix}.$$

s is a real-valued scaling factor, and P is a 3 by 4 perspective transformation matrix. Specifically, A is the 3 by 3 intrinsic parameter matrix. $[R|t]$ is the 3 by 4 joint rotation-translation matrix, or extrinsic parameter matrix, where R specifies the rotation and t specifies the translation. The people’s height $z = 1750mm$ is the same as in MVMS [23]. The projected features are further fused via a view max-pooling step. After that, a reasonable selection of feature information from different perspectives for fusion can effectively help model prediction. Finally, the fused multi-view features are fed into the multi-view decoder for predicting the people’s occupancy map on the ground.

As to the baseline method’s training loss, we adopt the **optimal transport** loss, which utilizes point maps as supervision in the single-view localization tasks [70] for multi-view crowd localization. We denote x as the predicted density map, where x_i is the density of pixels. And, we denote y as the ground-truth dot map, where $y_j \in \{0, 1\}$ indicates there is a person at location y_j . The optimal transport loss is as follows.

$$\mathcal{L}_C^T = \min_{\mathbf{P} \in \mathcal{R}_+^{n \times m}} \langle \mathbf{C}, \mathbf{P} \rangle - \varepsilon H(\mathbf{P}) + \tau \| P \mathbf{1}_m - a \|_2^2 + \tau \| P^T \mathbf{1}_n - b \|_1,$$

where $P \in \mathcal{R}_+^{n \times m}$ is the transport plan matrix, which indicates each density x_i of predicted density map to y_i of the ground-truth dot map for measuring the cost. $C \in \mathcal{R}_+^{n \times m}$ is the transport cost matrix, where C_{ij} measures the cost of moving the predicted density at x_i to y_j . We use Euclidean distance between points as a cost function: $C_{ij} = c(x_i, y_j) = \exp(\|x_i - y_j\|)$. The second term $H(\mathbf{P}) = -\sum_{ij} \mathbf{P}_{ij} \log \mathbf{P}_{ij}$ is the entropic regularization term. The remaining term is ensuring all predicted density values have a corresponding annotation, and all ground-truth points are used in the transport plan, respectively. Finally, τ and ε are weighted factors to adjust the weight of the last three terms.

4.1.2 Experiment Settings

Implementation details. The synthetic dataset contains 50 scenes in total, 30 scenes of which are used for training, 10 for validation, and the remaining 10 for testing. We randomly select 5 camera views 5 times and randomly choose 10 frames out of 200 of a scene in each iteration. For evaluation, we randomly select 5 views for 5 times per frame of each scene. The experimental settings remain consistent with all methods. We use a patch training method as in [5], with a resolution of 200×200 , and each example contains 3 patches. Each grid in the ground plane map stands for 0.2 meters in the real world. During training, we first train the 2D detection task as the pretraining

Table 3: The results of multi-view crowd localization methods on the SynMVCrowd dataset. Our baseline method, Baseline (OT) outperforms all comparisons.

Method	MODA \uparrow	MODP \uparrow	Precision \uparrow	Recall \uparrow	F1_score \uparrow
MVDet [6]	27.0	52.2	72.2	43.9	54.6
SHOT [11]	32.5	52.6	74.5	49.3	59.3
MVDeTr [12]	35.6	69.7	95.4	37.4	53.7
3DROM [1]	24.2	59.2	86.1	28.8	43.2
SVCW [13]	35.8	55.6	75.8	51.7	61.4
MVOT [32]	45.5	66.3	83.4	56.9	67.6
TrackTacular [33]	45.8	71.1	92.6	49.8	64.8
Baseline (MSE)	34.6	74.5	92.9	37.4	53.4
Baseline (OT)	49.6	70.2	88.6	57.0	69.4

for the feature extraction subnet, where only head annotations in 2D images are used in training. Then, the multi-view decoding subnet and feature extraction subnet are trained together, where the loss term weight follows [6]. In the end, we use the whole image to evaluate the model’s performance. Two Nvidia RTX3090 GPUs are used to conduct all experiments. In this work, the proposed model is trained with MSE loss or OT loss, respectively. We trained the model for approximately 200 epochs, using Stochastic Gradient Descent (SGD) as the optimizer. Our learning rate was set to a maximum value of 0.0001, and we employed the PyTorch scheduler “LambdaLR”. We also used a momentum of 0.9 and a weight decay of 1e-4.

Comparisons. We compare the mean square error loss (MSE) and the optimal transport loss on the baseline model, denoted as ‘Baseline (MSE)’ and ‘Baseline (OT)’. In addition, the proposed baseline method is also compared with seven state-of-the-art multi-view crowd localization methods, including MVDet [6], SHOT [11], MVDeTr [12], 3DROM [1], SVCW [13], MVOT [32], and TrackTacular [33] on the proposed SynMVCrowd benchmark.

Evaluation metrics. We use 5 metrics to evaluate the localization precision: Multiple Object Detection Precision (MODP), Multiple Object Detection Accuracy (MODA), Precision, Recall, and F1_score. First, we count the number of True Positives (TP), False Positives (FP), and False Negatives (FN) to compute the metrics. The formulas of metric can be formulated as follows: $MODA = 1 - (FP + FN) / (TP + FN)$, $MODP = (\sum(1 - d[d < t] / t)) / TP$, $Precision = TP / (TP + FP)$, $Recall = TP / (TP + FN)$ and $F1_score = 2Precision * Recall / (Precision + Recall)$. F1_score is a balance of *Precision* and *Recall*. In MODP, d represents the Euclidean distance between each predicted point and the GT point, and t represents the distance threshold.

4.1.3 Experiment Results

Result Analysis The results of SOTA methods and the proposed baselines on SynMVCrowd are presented in Table 3, which shows all SOTAs perform badly with lower MODA and F1_score than the proposed Baseline (OT) trained with optimal transport loss. SHOT achieves the second-highest F1_score and is better than MVDet, indicating the effectiveness of the multi-height fusion module in SHOT. MVDeTr achieves the second-highest MODA and the highest MODP among all methods, which proves

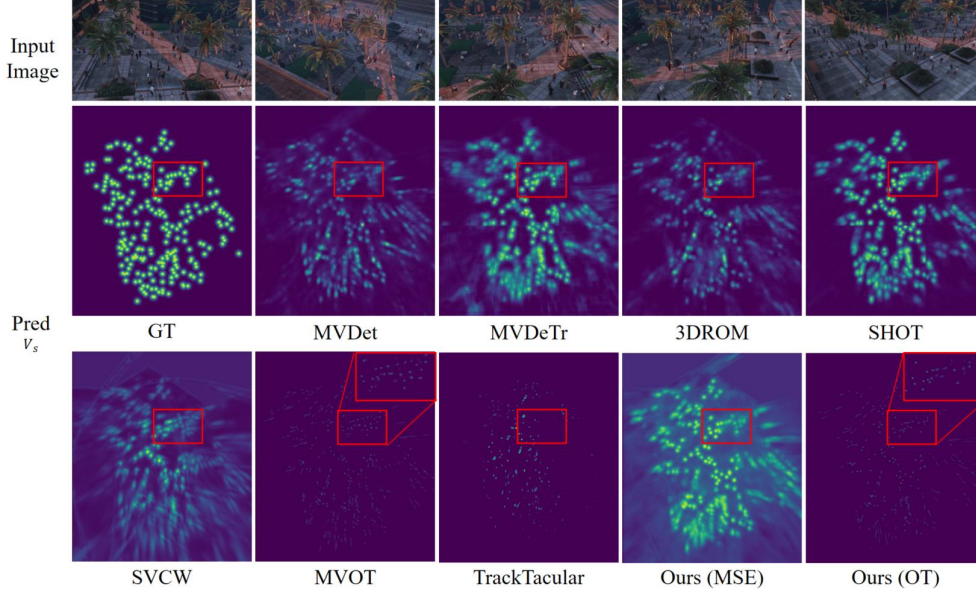


Fig. 9: The visualization results of multi-view crowd localization: the first row is the camera view input, and the second row is the corresponding ground truth (GT) and prediction results.

the advantage of the multi-view deformable fusion layer. 3DROM doesn't perform well because 3DROM is a data augmentation method for handling overfitting issues, but SynMVCrowd is already a large dataset. SVCW [13] and TrackTacular [33] are the latest methods, since the SynMVCrowd dataset contains much more complicated scenarios than other datasets, and their design doesn't achieve satisfying performance on SynMVCrowd. MVOT uses a more precise point-supervision loss instead of the MSE Gaussian density map, and thus achieves higher performance than other methods. But the proposed baseline model still outperforms all comparisons on the SynMVCrowd dataset, demonstrating the effectiveness of the model under large scenes. These experiments all indicate that SynMVCrowd is a very challenging platform for multi-view crowd localization evaluation. See visualization results in Fig. 9.

4.1.4 Generalization to Novel Scenes

We also added generalization experiments to the multi-view crowd localization datasets Wildtrack and MultiviewX, as seen in Table 4. In Table 4, we compare the results of SOTA multi-view crowd localization methods trained and tested on Wildtrack or MultiviewX solely, with Our Baseline methods' results trained on SynMVCrowd and tested on Wildtrack or MultiviewX. It concludes that our model trained on SynMVCrowd can be well applied to new scenes with simple finetuning, which is fast and achieves comparable performance to SOTAs, eg, MVDet. With the extra domain technique, the performance can be further promoted and outperform MVDet. Even

Table 4: Comparison of the multi-view people detection performance on Wildtrack and MultiviewX using 5 metrics. All comparison methods train and test on Wildtrack or MultiviewX (single scene), while ours are trained on SynMVCrowd and finetuned on Wildtrack or MultiviewX or with the domain adaptation technique.

Dataset Method	Wildtrack					MultiviewX				
	MA.	MP.	P.	R.	F1.	MA.	MP.	P.	R.	F1.
RCNN [71]	11.3	18.4	68	43	52.7	18.7	46.4	63.5	43.9	51.9
POM-CNN [72]	23.2	30.5	75	55	63.5	-	-	-	-	-
DeepMCD [30]	67.8	64.2	85	82	83.5	70.0	73.0	85.7	83.3	84.5
DeepOcc. [29]	74.1	53.8	95	80	86.9	75.2	54.7	97.8	80.2	88.1
Volumetric [7]	88.6	73.8	95.3	93.2	94.2	84.2	80.3	97.5	86.4	91.6
MVDet [6]	88.2	75.7	94.7	93.6	94.1	83.9	79.6	96.8	86.7	91.5
SHOT [11]	90.2	76.5	96.1	94.0	95.0	88.3	82.0	96.6	91.5	94.0
MVDeTr [12]	91.5	82.1	97.4	94.0	95.7	93.7	91.3	99.5	94.2	97.8
3DROM [1]	93.5	75.9	97.2	96.2	96.7	95.0	84.9	99.0	96.1	97.5
MVOT [32]	92.1	81.3	94.5	97.8	96.1	96.7	86.1	98.8	97.9	98.3
EarlyBird [73]	91.2	81.8	94.9	96.3	95.6	94.2	90.1	98.6	95.7	97.1
TrackTacular [33]	92.1	76.2	97.0	95.1	96.0	96.5	75.0	99.4	97.1	98.2
POV-MVD [74]	93.6	82.4	96.6	97.0	96.8	97.3	95.0	99.5	97.9	98.7
Baseline (test)	31.9	48.5	78.4	44.1	56.5	25.4	52.0	62.6	62.0	62.4
Baseline (10%)	55.0	68.3	77.6	77.3	77.5	66.4	73.0	92.6	72.1	81.1
Baseline (30%)	67.8	71.1	83.2	84.9	84.0	74.0	75.6	92.5	80.5	86.1
Baseline (100%)	85.9	76.5	94.1	91.7	92.9	84.8	84.7	99.1	85.6	91.8
Baseline (10%+DA)	63.2	73.6	82.4	83.9	83.2	72.9	78.2	94.1	78.5	85.7
Baseline (30%+DA)	75.3	78.4	89.7	89.2	89.4	79.8	81.2	95.9	86.2	90.7
Baseline (100%+DA)	88.7	81.3	95.3	93.9	94.6	87.6	87.9	99.4	89.0	93.9

though there is a performance gap between our domain transferring results and single-scene results of the latest SOTAs, such as 3DROM, POV-MVD, etc, SynMVCrowd still provides a new platform for studying better domain transferring methods for the multi-view localization tasks.

4.2 Multi-view Crowd Counting

4.2.1 Methods

As to multi-view crowd counting, we evaluate and compare the latest SOTA methods on SynMVCrowd, including MVMS [75], MVMSR [75], CVCS backbone [5], CVCS [5], and 3DCounting [24]. Besides, we also adopt the proposed baseline method (as in Sec. 4.1) for multi-view crowd counting on SynMVCrowd, where a different Gaussian kernel is used to generate ground truth density maps whose sum is equal to the number of persons in the scenario. Two losses, MSE and OT losses, are also enforced in the baseline model, respectively.

4.2.2 Evaluation Metrics

For multi-view counting evaluation, we use three metrics: Mean Absolute Error (MAE), Mean Squared Error (MSE), and mean Normalized Absolute Error (NAE) of the predicted and ground-truth crowd numbers. The formulas are defined as follows: $MAE = \sum(|z_i - \hat{z}_i|/N)$, $MSE = \sqrt{\sum(z_i - \hat{z}_i)^2/N}$, $NAE = \sum|z_i - \hat{z}_i|/(z_i * N)$,

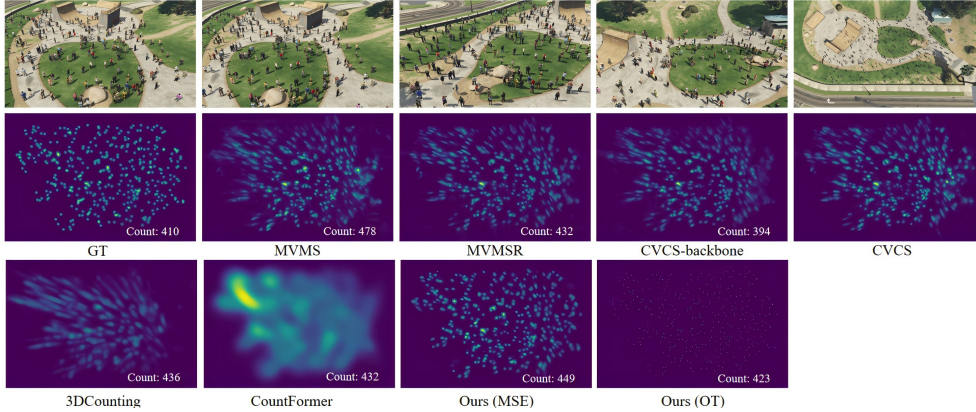


Fig. 10: The visualization results of multi-view crowd counting: the first row is the camera view input, and the second is the corresponding ground truth (GT) and prediction results.

Table 5: The results of multi-view crowd counting methods on the SynMVCrowd dataset.

Method	MAE ↓	NAE ↓	MSE ↓
MVMS [75]	81.51	0.173	102.74
MVMSR [75]	70.60	0.143	93.26
CVCS backbone [5]	72.50	0.154	93.99
CVCS [5]	67.74	0.139	89.31
3DCounting [24]	74.63	0.171	101.30
CountFormer [14]	56.30	0.117	79.30
Baseline (MSE)	68.79	0.158	92.04
Baseline (OT)	50.20	0.104	68.19

where N is the number of images, z_i is the actual number of people existed in the i -th image, and \hat{z}_i indicates the predicted number of people in the i -th image.

4.2.3 Experiment Results

Result analysis. The results of state-of-the-art multi-view crowd counting methods and the baseline method on SynMVCrowd are shown in Table 5, and the visualization results are shown in Fig 10. MVMS achieves worse performance than MVMSR, showing that the rotation selection layer in MVMSR can effectively alleviate the projection distortion. CVCS achieves better performance than the CVCS backbone and MVMSR, indicating the fusion effectiveness of the camera selection module in CVCS. The proposed baseline method ‘Baseline (OT)’ achieves the best performance among all methods. Overall, all multi-view crowd counting methods generally perform much worse on SynMVCrowd than on other multi-view datasets. Thus, SynMVCrowd is a more difficult benchmark for the multi-view counting task, and more methods that could handle large crowd numbers with more scene and view variations are in demand in this area.

Table 6: The multi-view counting and localization performance comparison of using different feature extraction backbones in the Baseline (OT) model, which is trained on the SynMVCrowd dataset with 5 views as input.

Model	MAE↓	MSE↓	NAE↓	MODA↑	MODP↑	Precision↑	Recall↑	F1_score↑
VGG19	59.04	83.00	0.155	43.8	69.6	88.4	51.6	65.0
ResNet18	50.20	68.19	0.104	49.6	70.2	88.6	57.0	69.4
Transformer	66.23	92.84	0.211	39.5	62.1	80.1	48.3	60.3

Table 7: Testing the baseline model on the multi-view counting task under different camera view numbers.

Models	test views	MAE↓	MSE↓	NAE↓
CountFormer	3	47.71	65.24	0.151
	5	56.30	79.30	0.117
	7	71.47	95.95	0.158
	9	77.82	102.96	0.164
Baseline (OT)	3	57.97	69.00	0.137
	5	50.20	68.19	0.104
	7	46.25	59.57	0.113
	9	42.46	58.34	0.106

Backbone model ablation study. We have conducted an ablation study on the Baseline (OT)’s model architecture by using different single-view feature extraction backbones for the multi-view counting and localization, eg, ResNet18 [76], Transformer [77], as in Table 6. Each model is trained on SynMVCrowd with 5 views as input, while keeping all other settings the same. From the table, we conclude that the best results are achieved by using ResNet18. The possible reason is that ResNet18 pre-trained weights provide more useful information compared to VGG19, and it seems the transformer-based model consists of too many deep layers and cannot perform counting and localization tasks well on the dataset. Thus, we use ResNet18 as the main backbone for the proposed baseline model.

Test camera number ablation study. We conducted an ablation study on the different numbers of input camera views in Table 7. The Baseline (OT) and CountFormer model is trained on the SynMVCrowd dataset with 5 input views and is tested with 3-9 camera views in Table 7. We can conclude that the model performance is steadily increased with more camera views, since more camera views can cover the scenes well. In contrast, CountFormer’s performance decreases a lot when the camera view number increases, indicating the model is not robust to variable input camera views on the SynMVCrowd dataset, since the multi-view prediction error is accumulated with more cameras. It also demonstrates the proposed baseline model’s advantages in fusing multi-camera information under different testing camera views.

Spatial feature selection module ablation study. We have conducted an ablation study on the baseline model with/without the spatial module, as shown in Table 8. We conclude that, no matter using MSE or OT loss, the model with the

Table 8: Performance Comparison of baseline model with/without spatial feature selection module using MSE or OT loss.

Loss	Module	MAE↓	MSE↓	NAE↓	MODA↑	MODP↑	Precision↑	Recall↑	F1_score↑
MSE	Without	74.33	97.52	0.236	31.9	74.8	94.1	34.0	49.9
	With	68.79	92.04	0.158	34.6	74.5	92.9	37.4	53.4
OT	Without	52.94	78.21	0.105	46.7	69.7	87.9	54.1	67.0
	With	50.20	68.19	0.104	49.6	70.2	88.6	57.0	69.4

Table 9: The performance comparison of the different pitch ranges.

Pitch	MAE↓	MSE↓	NAE↓	MODA↑	MODP↑	Precision↑	Recall↑	F1_score↑
[-90, -60)	48.19	67.00	0.100	46.0	64.9	85.0	55.9	67.4
[-60, -30)	49.62	68.29	0.105	45.6	67.8	84.8	55.6	67.2
[-30, 0]	55.97	76.03	0.118	42.9	66.7	83.4	53.6	65.2

Table 10: Computation statistic comparison of different methods.

Methods	Parameters (MB)	FLOPs (G)	Memory (MB)
MVDet [6]	30.10	910.44	114.85
SHOT [11]	19.14	1230.24	73.04
MVDeTr [12]	12.78	148.30	48.78
3DROM [24]	32.46	1012.36	123.86
SVCW [13]	25.71	3413.13	98.12
MVOT [32]	18.59	349.73	70.95
TrackTacular [33]	30.50	922.54	116.43
Baseline	18.63	349.93	71.09

spatial feature selection outperforms the one without it on both multi-view counting and localization tasks. It demonstrates the effectiveness of the spatial feature selection module for selecting useful features in better multi-view fusion.

Camera angle influence. We also provide an ablation study on the camera angle’s influence on the crowd counting and localization performance in Table 9. We divide the vertical pitch into three parts for multi-view counting and localization performance analysis: [-90,-60), [-60, -30), and [-30, 0]. Each camera angle group’s multi-view crowd counting and localization results are shown in Table 9. For each sample in the test set, we randomly select 5 camera views of each frame, where the pitch angle of each view falls within the corresponding angle group. Apparently, the camera pitch significantly influences the performance of multi-view crowd counting and localization. The performance of both counting and detection consistently declines as the camera pitch shifts from downward to frontal views. This trend indicates that frontal perspectives introduce greater occlusion and scale variation, making accurate localization and density estimation more challenging compared to downward-oriented angles.

Table 11: The multi-view crowd counting domain adaptation (DA) results on the CityStreet dataset and the PETS2009 dataset.

Training	Dataset Method	CityStreet			PETS2009		
		MAE ↓	NAE ↓	MSE ↓	MAE ↓	NAE ↓	MSE ↓
Single-scene	Dmap_wtd [21]	11.10	0.121	-	7.51	0.261	-
	Dect+ReID [23]	27.60	0.385	-	9.41	0.289	-
	LateFusion [23]	8.12	0.097	-	3.92	0.138	-
	EarlyFusion [23]	8.10	0.096	-	5.43	0.199	-
	MVMS (FCN-7) [23]	8.01	0.096	10.05	3.49	0.124	4.83
	MVMS (CSRNet) [75]	7.36	0.096	9.02	3.99	0.140	5.26
	MVMSR (CSRNet) [75]	6.98	0.086	8.49	4.15	0.151	5.60
	3DCounting [24]	8.01	0.096	-	3.15	0.113	-
Cross-scene	CountFormer [14]	4.72	0.058	-	0.74	0.030	-
	Baseline (test)	80.92	0.944	89.43	27.92	0.868	29.10
	Baseline (10%)	13.95	0.155	17.37	9.60	0.324	11.43
	Baseline (30%)	10.55	0.132	13.43	9.37	0.317	11.16
	Baseline (100%)	7.24	0.085	8.96	3.46	0.116	4.57
	Baseline (10%+DA)	12.67	0.152	16.24	5.31	0.177	6.46
	Baseline (30%+DA)	10.02	0.130	12.16	4.26	0.147	5.49
	Baseline (100%+DA)	6.85	0.083	8.46	3.29	0.112	4.54

Computation statistic comparison. Besides, we compare the models’ computation statistics, parameter number, FLOPs, and model parameter memory size, as seen in Table 10. Baseline model parameter is smaller than MVDet, due to a smaller feature dimension being used. 3DROM, TrackTacular, and SVCW consume many more parameters because they need a more complicated architecture in the feature fusion or model supervision. It concludes that the baseline model’s parameter number is smaller than most methods, indicating its computational efficiency.

4.2.4 Generalization to Novel Scenes

Table 11 presents the generalization performance of the multi-view counting baseline method trained on SynMVCrowd with OT loss to new scenes CityStreet [23] and PETS2009 [9]. ‘Baseline (test)’ means testing the ‘Baseline’ model (trained on SynMVCrowd) directly on the CityStreet dataset; ‘Baseline (X%)’ means fine-tuning the ‘Baseline (OT)’ model on the new datasets with 10%, 30%, and 100% annotations, respectively; ‘Baseline (X%+DA)’ means adapting the ‘Baseline (OT)’ model to the new datasets with domain adaption approaches and X% annotations. We train ‘Baseline (X%+DA)’ with two steps. First, we apply single-image unsupervised domain adaptation to fine-tune the trained model’s feature extractor as in [78]. In particular, we add a feature discriminator behind the feature extractor of the baseline model to reduce the domain gap between the two datasets. During the fine-tuning stage, both the real and synthetic images are input into the model, and then the features are fed into the discriminator for classification. Next, we input the extracted features into a single-view decoder, expecting that the feature extractor can learn useful feature information. In this process, we only use the annotation of the synthetic dataset. Second, we fix the trained feature extractor and only train the multi-view feature decoder by using X% CityStreet or PETS2009 annotations and synthetic annotations.

According to Table 11, there is a large performance gap between the cross-scene testing ‘Baseline (test)’ and the single-scene methods, such as MVMS [23] or MVMSR

[75], due to the domain gap between the real and synthetic scenes. However, the gap could be largely reduced with a small set of labels for fine-tuning and could be reduced further with domain adaptation techniques (see ‘Baseline (30%)’ and ‘Baseline (100%)’, comparing with ‘Baseline (30%+DA)’ and ‘Baseline (100%+DA)’). With fully-supervised finetuning and simple domain techniques, the baseline model trained on SynMVCrowd can also achieve comparable and better performance compared to 3DCounting and MVMSR, even though still lower than CountFormer. In the future, the domain adaptation methods will be a key topic in multi-view crowd counting, and our SynMVCrowd benchmark could serve as an important platform.

4.3 Single-image Counting and Localization

4.3.1 Methods

In addition to multi-view crowd counting and localization, SynMVCrowd could also serve as a challenging platform for evaluating and comparing single-image counting and localization tasks. We test and compare 7 mainstream single-image counting and localization methods with publicly available codes on SynMVCrowd: CSRNet [15], DM-Count [16], NoisyCC [79], GLoss [70] and P2PNet [17], CLTR [80], STEERER [81], GramFormer [55] and FreeLunch [56]. Besides, we use domain adaptation techniques to improve the baseline counting model’s cross-scene generalization performance trained on SynMVCrowd and compare it with the performance of single-scene methods. We use MAE, MSE, and NAE to evaluate the counting performance and Precision, Recall, and F1_score to evaluate the localization performance (as in the metrics of Sec. 4.1).

4.3.2 Experiment settings

For SynMVCrowd, the training set, the validation set, and the test set are also divided in a 3:1:1 ratio. During training, we randomly select 10 frames from the 200 frames of each scene per epoch for training. For evaluation, we select all frames of each scene in the test set. In the experiments, all the models are trained using the official codes and the default parameters. Besides, we randomly crop patches as inputs from images with a size of 512×512 as a way of data augmentation. The distance threshold for evaluating localization performance is 3 pixels for all methods. The ground truth density map for crowd counting is generated by a Gaussian kernel with a fixed size of 3. All experiments are conducted on one RTX3090 GPU.

4.3.3 Experiment results

Result analysis. We compare single-image crowd counting and localization methods on SynMVCrowd in Table 12. DM-Count performs the best among all methods in terms of crowd counting performance, and GLoss achieves slightly worse counting results than DM-Count, showing that the optimal transport method is quite robust for single-image crowd counting in different environments. As to single-image localization, STEERER [81] is the best one among all methods, and CLTR [80] achieves the second-best localization results. Compared to other density map regression methods

Table 12: The performance of single-image crowd counting and localization SOTA methods (**with code available**) on the SynMVCrowd dataset. We report all methods’ single-image counting and localization performance.

Method	MAE↓	MSE↓	Precision↑	Recall↑	F1_score↑
CSRNet [15]	21.84	36.58	50.77	69.59	58.71
DM-Count [16]	20.88	34.72	65.53	67.31	66.41
NoisyCC [79]	26.19	43.23	33.65	48.28	39.66
P2PNet [17]	61.74	115.03	80.59	67.62	73.54
GLoss [70]	21.37	40.36	79.37	70.63	74.75
CLTR [80]	23.86	38.53	85.47	66.02	74.50
STEERER [81]	22.81	41.75	88.83	67.79	76.70
GramFormer [55]	31.38	50.85	22.11	23.60	21.83
FreeLunch [56]	32.56	43.40	19.68	23.56	18.18

Table 13: The results on detailed evaluation granularity. We divide the scenes into 3 types regarding crowd numbers: ‘Sparse (0-399)’, ‘Medium (400-699)’, and ‘Congested (700-1000)’, and evaluate methods accordingly.

Method	Sparse (0-399)		Medium (400-699)		Congested (700-1000)	
	MAE ↓	MSE ↓	MAE ↓	MSE ↓	MAE ↓	MSE ↓
CSRNet [15]	14.92	23.69	27.06	42.75	45.17	64.85
DMCount [16]	18.23	29.76	25.00	41.00	35.34	56.58
NoisyCC [79]	20.45	31.01	29.78	43.77	47.61	68.95
P2PNet [17]	27.77	35.15	45.26	66.01	79.96	92.04
GLoss [70]	17.68	27.26	26.49	42.33	37.74	57.37
CLTR [80]	18.22	28.91	30.91	47.64	45.23	64.14
STEERER [81]	17.12	30.10	31.06	47.67	52.91	72.57
GramFormer [55]	24.38	36.98	41.34	68.77	81.35	125.93
FreeLunch [56]	28.96	38.30	41.08	54.79	66.79	82.93

(such as CSRNet [15], DM-Count [16], NoisyCC [79]), point supervision methods can achieve better localization results. In particular, NoisyCC achieves the worst localization results and the second-worst counting performance. The possible reason is that the annotation noise in SynMVCrowd is rare due to no human labeling process, which reduces NoisyCC’s noise modeling effectiveness. CSRNet achieves slightly worse counting results than DM-Count and GLoss, but CSRNet achieves much worse localization results, because DM-Count and GLoss use optimal transport with better localization ability than the density maps supervision of CSRNet.

Surprisingly, P2PNet achieves the worst counting results and the third-best localization performance. The reason may be that P2PNet is a point proposal prediction method, and its prediction results are more likely to be affected by factors such as light and camera placement angle changes. In the case of the latest works, GramFormer [55] and FreeLunch [56], both fail to deliver promising results. GramFormer requires controlling the head width of datasets, while FreeLunch relies on thermal maps as ground

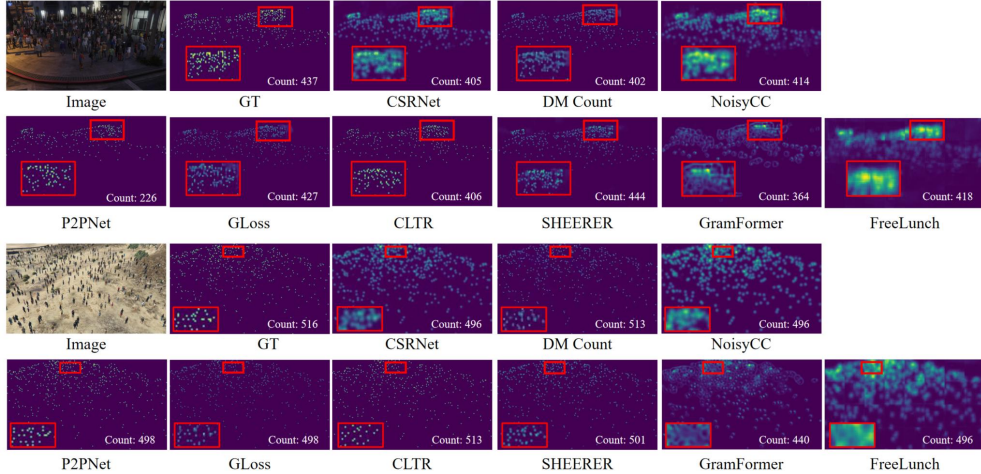


Fig. 11: The visualization results of single-image crowd counting and localization.

truth. Since SynMVCrowd does not meet these specific requirements, we set the head width to a fixed value of 5 pixels and omitted the corresponding thermal map loss. This is the primary reason why the results of these methods are relatively worse compared to others. In SynMVCrowd, we have more horizontal camera views and around 50,000 out of 5.3 million images under low illumination conditions, whose numbers are more than any existing single-image dataset. Thus, it is a rather challenging dataset. Fig. 11 demonstrates the visualization results of all comparisons.

Count granularity. Besides, we also evaluate all methods of higher granularity in Table 13. In detail, we divide the scenes into 3 types regarding crowd numbers: Sparse (0-399), Medium (400-699), and Congested (700-1000), and evaluate methods accordingly. It shows P2PNet [17] performs badly in Congested scenes, where SynMVCrowd contains many scenes with large crowd numbers (700-1000); Even though CSRNet [15] is old, it is good on sparse scenes; DMCount [16] is better in congested scenes, thus it shows the best counting performance.

4.3.4 Generalization to Novel Scenes

To evaluate the effectiveness of our proposed dataset, we conduct experiments to present the generalization performance of the baseline counting method trained on SynMVCrowd to novel scenes. The single-image domain transferring model’s detailed structure is shown in Fig. 12 and Table 14.

The single-image feature extractor is based on VGG19, and the single-image decoder is the same as in DM-Count [16]. When transferring the baseline to novel new scenes, we randomly crop patches as inputs from images with a size of 512×512 . After the single-image feature extractor, we obtain the image features of size $[1, 512, 64, 64]$, which contains an up-sampling operation with the size of two scale factors. In discrimination, we first transform the input image features into features of size $[1, 8, 64, 64]$ through the convolutional layer. Next, the features are converted into a

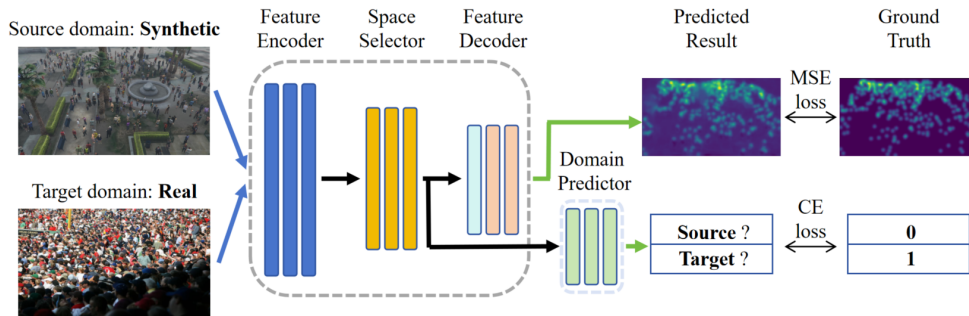


Fig. 12: Architecture of the domain adaptation network for single-image crowd counting. The model takes synthetic (source) and real (target) images as input. Features are encoded and selected, then processed through two branches: 1) A decoder producing density maps, supervised by MSE loss against ground truth; 2) A domain predictor distinguishing source from target features using cross-entropy (CE) loss. This adversarial training aligns feature distributions across domains to improve generalization.

Table 14: The single-image baseline for domain adaptation. The single-image baseline includes a single-image feature extractor, a single-image decoder, and a discriminator. The Filter dimensions are input channels, output channels, and filter size ($w \times h$).

Single-image baseline	
Single-image feature extractor	
Layer	Feature Extractor
Layer	UpSampling
Single-image decoder	
Layer	Filter
conv 1	$512 \times 256 \times 3 \times 3$, relu
conv 2	$256 \times 128 \times 3 \times 3$, relu
conv 3	$128 \times 1 \times 1 \times 1$
Discriminator	
Layer	Filter
conv	$512 \times 8 \times 1 \times 1$
linear1	32768×1024 , relu
linear2	1024×1024 , relu
linear3	1024×2

two-dimensional vector of $[1, 8 \times 64 \times 64]$, which is then input into the fully connected layer to obtain category predictions.

Table 15 reports the results of the single-scene methods [15, 16, 70, 82, 83] and our cross-scene methods on ShanghaiTech A and ShanghaiTech B [2]. ‘Test (GCC)’ means testing the baseline counting model trained on GCC dataset (a synthetic single-image counting dataset [10]) directly on ShanghaiTech A and ShanghaiTech B; ‘Test (SynMVCrowd)’ means testing the baseline model trained on our proposed SynMVCrowd dataset directly on above two datasets; ‘SE Cycle GAN (GCC)’ represents the SE Cycle GAN method in [10] trained on GCC for domain adaptation to above two datasets; ‘UDA (SynMVCrowd)’ means adapting the baseline model trained on SynMVCrowd to above two datasets with a unsupervised domain adaption technique, which is as follows.

For ‘UDA (SynMVCrowd)’, we use a domain adversarial method [78] to reduce the domain gap between the two different datasets. The baseline counting model contains a backbone module to extract multi-scale features and a density map regression head. ‘UDA (SynMVCrowd)’ contains an extra classification head to distinguish synthetic and real images, based on the baseline counting model. During the training

Table 15: The single-image crowd counting domain adaptation results on the ShanghaiTech A and B dataset.

Training	Dataset Method	SHA		SHB	
		MAE ↓	MSE ↓	MAE ↓	MSE ↓
Single-scene	MCNN [82]	110.20	173.20	26.40	41.30
	CSRNet [15]	68.20	115.00	10.60	16.00
	DM-Count [16]	59.70	95.70	7.40	11.80
	GLoss [70]	61.30	95.40	7.30	11.70
	GauNet [83]	54.80	89.10	6.20	9.90
	PET [84]	49.3	78.70	6.10	9.60
	APGCC [85]	48.80	76.70	5.60	8.70
	DiffusionLoc [86]	50.30	79.10	5.40	8.50
Cross-scene	Test (GCC)	160.80	216.50	22.80	30.60
	Test (SynMVCrowd)	187.70	291.90	18.10	28.30
	SE Cycle GAN (GCC)	123.40	193.40	19.90	28.30
	UDA (SynMVCrowd)	118.70	182.90	11.20	18.40

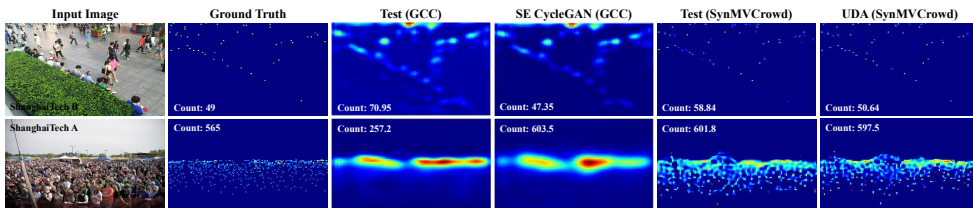


Fig. 13: The domain adaptation visualization results of single-image crowd counting on ShanghaiTech B and ShanghaiTech A.

process, all dataset images are fed into the backbone module, and then we get the extracted features. Next, we input the features into the regression head, expecting to obtain a reliable single-view crowd density prediction by only using synthetic annotations for supervision. In addition, we use the classification head to classify features to encourage the backbone module to learn domain-invariant feature information from the different domains.

According to Table 15, due to the domain gap between real and synthetic scenarios, there is a gap among the performance of the cross-scene test (‘Test (GCC)’, ‘Test (SynMVCrowd)’) and the single-scene SOTA methods. However, this gap can be reduced by unsupervised domain adaptation techniques, as in ‘UDA (SynMVCrowd)’. The visualization results are shown in Fig. 13. From the results, ‘Test (SynMVCrowd)’ achieves a better counting performance than ‘Test (GCC)’. Besides, ‘UDA (SynMVCrowd)’ achieves a much lower MAE metric score of 11.2 compared to ‘SE Cycle GAN (GCC)’, which scores 19.9. In addition, we present the generalization results on ShanghaiTech A (more crowds) in Table 15 left. We conclude that the model trained on our dataset with a simple unsupervised method (UDA) could achieve better performance compared to utilizing a specially designed domain transferring method, SE Cycle GAN trained on the GCC dataset. Both the above results demonstrate that the larger number of images in our dataset can cover more scenarios in practice. In conclusion, SynMVCrowd can advance related research and serve as a challenging benchmark for single-image counting and localization tasks.

Table 16: The single-image crowd counting domain adaptation results on UCF-CC-50 and Mall datasets. Comparisons are all trained and tested on the same datasets, while ours is trained on SynMVCrowd and tested on UCF-CC-50 or Mall.

Datasets	UCF-CC-50			MALL		
	MAE↓	NAE↓	MSE↓	MAE↓	NAE↓	MSE↓
Crowd-CNN [87]	466.90	-	498.60	1.83	-	2.76
MCNN [82]	377.60	-	509.10	2.74	-	13.50
CSRNet [15]	266.10	-	397.50	-	-	-
DecideNet [88]	361.80	-	493.50	1.53	-	1.89
IG-CNN [89]	419.60	-	541.80	2.39	-	9.14
ST-CNN [90]	229.40	-	325.60	4.03	-	5.87
DM-Count [16]	211.00	-	291.50	-	-	-
P2PNet [17]	172.72	-	256.18	-	-	-
U-ASD Net [91]	232.30	-	217.80	1.80	-	2.20
GRGAF-ST [92]	-	-	-	1.61	-	2.07
PET [84]	159.90	-	223.70	-	-	-
CL-DCNN [93]	181.80	-	240.60	1.55	-	2.01
APGCC [85]	154.80	-	205.50	-	-	-
DiffusionLoc [86]	135.30	-	201.70	-	-	-
Baseline(test)	1052.04	0.763	1367.31	21.67	0.729	21.95
Baseline(10%)	278.52	0.271	339.40	1.99	0.065	2.55
Baseline(30%)	266.28	0.260	329.19	1.67	0.055	2.13
Baseline(100%)	249.67	0.250	315.52	1.39	0.046	1.81
Baseline(10%+DA)	229.82	0.237	315.49	1.84	0.061	2.33
Baseline(30%+DA)	214.57	0.231	284.40	1.41	0.046	1.80
Baseline(100%+DA)	202.34	0.224	265.14	1.34	0.044	1.74

Besides, we also perform the single-image counting domain transferring experiments on UCF-CC-50 [62] and Mall [64], whose results are shown in Table 16. The model trained on SynMVCrowd cannot perform well by directly testing on novel new scenes UCF-CC-50 and Mall datasets, since the domain gap between SynMVCrowd and the two datasets is quite large. But, with more labeled target dataset annotations for finetuning, the performance on both datasets increased steadily, and with 100% finetuning annotations, our domain transferring results already outperform existing SOTA methods on Mall. With further domain adaptation techniques (100%+DA), the performance can be further improved. On UCF-CC-50, since the crowd count in the images varies from tens to thousands, there is a much larger domain gap with SynMVCrowd, and thus the performance is lower than recent single-scene SOTAs, but we still achieve better performance than DM-Count and U-ASD Net. Since SynMVCrowd contains various scenes, camera views, and environmental conditions, it can serve as an important benchmark for single-image counting and domain transferring tasks.

5 Discussion and Conclusion

In this paper, we propose a synthetic crowd benchmark called SynMVCrowd for multi-view and single-image crowd counting and localization tasks. As far as we know, SynMVCrowd is the largest synthetic dataset for multi-view and single-image crowd vision tasks, which consists of a large number of crowd scenes, camera views, and frames with a large crowd number in each scene. Several state-of-the-art multi-view and single-image crowd counting and localization methods are evaluated and compared on the benchmark. Besides, we propose strong baselines and achieve better performance than comparisons, and the experiments show SynMVCrowd can be applied to novel scenes with domain adaptation techniques. It proves that SynMVCrowd can serve as a challenging platform for more practical research for multi-view and single-image crowd counting and localization. In addition to multi-view and single-image counting and localization tasks, the proposed dataset can also be used in tasks like crowd segmentation, 2D/3D pose estimation, camera calibrations, novel view synthesis, or large-scene 3D reconstruction, *etc.*

Acknowledgements

This work was supported in parts by Guangdong S&T Program (2024B0101050004), NSFC (62202312), ICFCRT (W2441020), Shenzhen Science and Technology Program (KJZD20240903100022028, KQTD20210811090044003, RCJC20200714114435012), and Scientific Foundation for Youth Scholars of Shenzhen University.

Declarations

Ethical consideration. We generate a synthetic multi-view image dataset as a challenging platform for multi-view and single-image counting and localization, with no real persons recorded or used in the model training and testing, which shall reduce the ethical issues for the public caused by crowd counting and localization tasks.

Data availability. The data supporting this study’s findings is available from the Visual Computing Research Center, Shenzhen University. The dataset is available from the authors upon reasonable request and with permission from the Visual Computing Research Center.

References

- [1] Qiu, R., Xu, M., Yan, Y., Smith, J.S., Yang, X.: 3d random occlusion and multi-layer projection for deep multi-camera pedestrian localization. In: European Conference on Computer Vision, pp. 695–710 (2022). Springer
- [2] Zhang, Y., Zhou, D., Chen, S., Gao, S., Ma, Y.: Single-image crowd counting via multi-column convolutional neural network. In: Proceedings of the IEEE Conference on Computer Vision and Pattern Recognition, pp. 589–597 (2016)
- [3] Ren, S., He, K., Girshick, R., Sun, J.: Faster r-cnn: Towards real-time object detection with region proposal networks. In: Advances in Neural Information Processing Systems, pp. 91–99 (2015)
- [4] Andriluka, M., Pishchulin, L., Gehler, P., Schiele, B.: 2d human pose estimation: New benchmark and state of the art analysis. In: Proceedings of the IEEE Conference on Computer Vision and Pattern Recognition, pp. 3686–3693 (2014)
- [5] Zhang, Q., Lin, W., Chan, A.B.: Cross-view cross-scene multi-view crowd counting. In: Proceedings of the IEEE Conference on Computer Vision and Pattern Recognition, pp. 557–567 (2021)
- [6] Hou, Y., Zheng, L., Gould, S.: Multiview detection with feature perspective transformation. In: Computer Vision—ECCV 2020: 16th European Conference, Glasgow, UK, August 23–28, 2020, Proceedings, Part VII 16, pp. 1–18 (2020). Springer
- [7] Iskakov, K., Burkov, E., Lempitsky, V., Malkov, Y.: Learnable triangulation of human pose. In: Proceedings of the IEEE/CVF International Conference on Computer Vision, pp. 7718–7727 (2019)
- [8] Chavdarova, T., Baqué, P., Bouquet, S., Maksai, A., Jose, C., Bagautdinov, T., Lettry, L., Fua, P., Van Gool, L., Fleuret, F.: Wildtrack: A multi-camera hd dataset for dense unscripted pedestrian detection. In: Proceedings of the IEEE Conference on Computer Vision and Pattern Recognition, pp. 5030–5039 (2018)
- [9] Ferryman, J., Shahrokni, A.: Pets2009: Dataset and challenge. In: 2009 Twelfth IEEE International Workshop on Performance Evaluation of Tracking and Surveillance, pp. 1–6 (2009). IEEE
- [10] Wang, Q., Gao, J., Lin, W., Yuan, Y.: Learning from synthetic data for crowd counting in the wild. In: Proceedings of the IEEE/CVF Conference on Computer Vision and Pattern Recognition, pp. 8198–8207 (2019)
- [11] Song, L., Wu, J., Yang, M., Zhang, Q., Li, Y., Yuan, J.: Stacked homography transformations for multi-view pedestrian detection. In: Proceedings of the IEEE/CVF International Conference on Computer Vision, pp. 6049–6057 (2021)

- [12] Hou, Y., Zheng, L.: Multiview detection with shadow transformer (and view-coherent data augmentation). In: Proceedings of the 29th ACM International Conference on Multimedia, pp. 1673–1682 (2021)
- [13] Zhang, Q., Gong, Y., Chen, D., Chan, A.B., Huang, H.: Multi-view people detection in large scenes via supervised view-wise contribution weighting. In: Proceedings of the AAAI Conference on Artificial Intelligence, vol. 38, pp. 7242–7250 (2024)
- [14] Mo, H., Zhang, X., Tan, J., Yang, C., Gu, Q., Hang, B., Ren, W.: Countformer: Multi-view crowd counting transformer. In: European Conference on Computer Vision, pp. 20–40 (2024). Springer
- [15] Li, Y., Zhang, X., Chen, D.: Csrnet: Dilated convolutional neural networks for understanding the highly congested scenes. In: Proceedings of the IEEE Conference on Computer Vision and Pattern Recognition, pp. 1091–1100 (2018)
- [16] Wang, B., Liu, H., Samaras, D., Nguyen, M.H.: Distribution matching for crowd counting. *Advances in neural information processing systems* **33**, 1595–1607 (2020)
- [17] Song, Q., Wang, C., Jiang, Z., Wang, Y., Tai, Y., Wang, C., Li, J., Huang, F., Wu, Y.: Rethinking counting and localization in crowds: A purely point-based framework. In: Proceedings of the IEEE/CVF International Conference on Computer Vision, pp. 3365–3374 (2021)
- [18] Ge, W., Collins, R.T.: Crowd detection with a multiview sampler. In: ECCV, pp. 324–337 (2010)
- [19] Li, J., Huang, L., Liu, C.: People counting across multiple cameras for intelligent video surveillance. In: IEEE Ninth International Conference on Advanced Video and Signal-Based Surveillance (AVSS), pp. 178–183 (2012). IEEE
- [20] Maddalena, L., Petrosino, A., Russo, F.: People counting by learning their appearance in a multi-view camera environment. *Pattern Recognition Letters* **36**, 125–134 (2014)
- [21] Ryan, D., Denman, S., Fookes, C., Sridharan, S.: Scene invariant multi camera crowd counting. *Pattern Recognition Letters* **44**(8), 98–112 (2014)
- [22] Tang, N., Lin, Y.Y., Weng, M.F., Liao, H.Y.: Cross-camera knowledge transfer for multiview people counting. *IEEE Transactions on Image Processing* **24**(1), 80–93 (2014)
- [23] Zhang, Q., Chan, A.B.: Wide-area crowd counting via ground-plane density maps and multi-view fusion cnns. In: CVPR, pp. 8297–8306 (2019)

- [24] Zhang, Q., Chan, A.B.: 3d crowd counting via multi-view fusion with 3d gaussian kernels. In: Proceedings of the AAAI Conference on Artificial Intelligence, vol. 34, pp. 12837–12844 (2020)
- [25] Zhang, Q., Chan, A.B.: Single-frame-based deep view synchronization for unsynchronized multicamera surveillance. *IEEE Transactions on Neural Networks and Learning Systems* **34**(12), 10653–10667 (2022)
- [26] Zhang, Q., Chan, A.B.: Calibration-free multi-view crowd counting. In: European Conference on Computer Vision, pp. 227–244 (2022). Springer
- [27] Li, B., Chen, D., Zhang, Q.: Wscf-mvcc: Weakly-supervised calibration-free multi-view crowd counting. In: Chinese Conference on Pattern Recognition and Computer Vision (PRCV), pp. 83–98 (2025). Springer
- [28] Zhang, Q., Gong, Y., Xie, Z., Wang, Z., Chan, A.B., Huang, H.: Semi-supervised multi-view crowd counting by ranking multi-view fusion models. arXiv preprint arXiv:2512.16243 (2025)
- [29] Baqué, P., Fleuret, F., Fua, P.: Deep occlusion reasoning for multi-camera multi-target detection. In: Proceedings of the IEEE International Conference on Computer Vision, pp. 271–279 (2017)
- [30] Chavdarova, T., Fleuret, F.: Deep multi-camera people detection. In: 2017 16th IEEE International Conference on Machine Learning and Applications (ICMLA), pp. 848–853 (2017). IEEE
- [31] Aung, S., Park, H., Jung, H., Cho, J.: Enhancing multi-view pedestrian detection through generalized 3d feature pulling, 1185–1194 (2024)
- [32] Zhang, Q., Zhang, K., Chan, A.B., Huang, H.: Mahalanobis distance-based multi-view optimal transport for multi-view crowd localization. In: European Conference on Computer Vision, pp. 19–36 (2024). Springer
- [33] Teepe, T., Wolters, P., Gilg, J., Herzog, F., Rigoll, G.: Lifting multi-view detection and tracking to the bird’s eye view. In: Proceedings of the IEEE/CVF Conference on Computer Vision and Pattern Recognition (CVPR) Workshops, pp. 667–676 (2024)
- [34] Daryani, A.E., Bhutta, M.U.M., Hernandez, B., Medeiros, H.: Camuvid: Calibration-free multi-view detection. In: Proceedings of the IEEE/CVF Conference on Computer Vision and Pattern Recognition (CVPR), pp. 1220–1229 (2025)
- [35] Ristani, E., Solera, F., Zou, R., Cucchiara, R., Tomasi, C.: Performance measures and a data set for multi-target, multi-camera tracking. In: European Conference on Computer Vision, pp. 17–35 (2016). Springer

- [36] Hafeezallah, A., Al-Dhamari, A., Abu-Bakar, S.A.R.: U-asd net: Supervised crowd counting based on semantic segmentation and adaptive scenario discovery. *IEEE Access* **9**, 127444–127459 (2021)
- [37] Xie, Y., Lu, Y., Wang, S.: Rsanet: Deep recurrent scale-aware network for crowd counting. In: *2020 IEEE International Conference on Image Processing (ICIP)*, pp. 1531–1535 (2020). IEEE
- [38] Liu, Y., Wen, Q., Chen, H., Liu, W., Qin, J., Han, G., He, S.: Crowd counting via cross-stage refinement networks. *IEEE Transactions on Image Processing* **29**, 6800–6812 (2020)
- [39] Liu, L., Qiu, Z., Li, G., Liu, S., Ouyang, W., Lin, L.: Crowd counting with deep structured scale integration network. In: *Proceedings of the IEEE/CVF International Conference on Computer Vision*, pp. 1774–1783 (2019)
- [40] Sindagi, V.A., Patel, V.M.: Multi-level bottom-top and top-bottom feature fusion for crowd counting. In: *Proceedings of the IEEE/CVF International Conference on Computer Vision*, pp. 1002–1012 (2019)
- [41] Huang, S., Li, X., Cheng, Z.-Q., Zhang, Z., Hauptmann, A.: Stacked pooling for boosting scale invariance of crowd counting. In: *ICASSP 2020 - 2020 IEEE International Conference on Acoustics, Speech and Signal Processing (ICASSP)*, pp. 2578–2582 (2020). <https://doi.org/10.1109/ICASSP40776.2020.9053070>
- [42] Cheng, Z.-Q., Li, J.-X., Dai, Q., Wu, X., He, J.-Y., Hauptmann, A.: Improving the learning of multi-column convolutional neural network for crowd counting. *arXiv preprint arXiv:1909.07608* (2019)
- [43] Ma, Y., Sanchez, V., Guha, T.: Fusioncount: efficient crowd counting via multi-scale feature fusion. In: *2022 IEEE International Conference on Image Processing (ICIP)*, pp. 3256–3260 (2022). IEEE
- [44] Chen, Y.e.a.: Learning discriminative features for crowd counting (2024)
- [45] Sindagi, V.A., Patel, V.M.: Generating high-quality crowd density maps using contextual pyramid cnns. In: *ICCV*, pp. 1879–1888 (2017)
- [46] Sam, D.B., Sajjan, N.N., Babu, R.V., Srinivasan, M.: Divide and grow: Capturing huge diversity in crowd images with incrementally growing cnn. In: *Proceedings of the IEEE Conference on Computer Vision and Pattern Recognition*, pp. 3618–3626 (2018)
- [47] Babu Sam, D., Surya, S., Venkatesh Babu, R.: Switching convolutional neural network for crowd counting. In: *Proceedings of the IEEE Conference on Computer Vision and Pattern Recognition*, pp. 5744–5752 (2017)

- [48] Liu, J., Gao, C., Meng, D., Hauptmann, A.G.: Decidenet: Counting varying density crowds through attention guided detection and density estimation. In: Proceedings of the IEEE Conference on Computer Vision and Pattern Recognition, pp. 5197–5206 (2018)
- [49] Xu, C., Qiu, K., Fu, J., Bai, S., Xu, Y., Bai, X.: Learn to scale: Generating multipolar normalized density maps for crowd counting. In: Proceedings of the IEEE/CVF International Conference on Computer Vision, pp. 8382–8390 (2019)
- [50] Xiong, H., Lu, H., Liu, C., Liu, L., Cao, Z., Shen, C.: From open set to closed set: Counting objects by spatial divide-and-conquer. In: Proceedings of the IEEE/CVF International Conference on Computer Vision, pp. 8362–8371 (2019)
- [51] Jiang, X., Zhang, L., Xu, M., Zhang, T., Lv, P., Zhou, B., Yang, X., Pang, Y.: Attention scaling for crowd counting. In: Proceedings of the IEEE/CVF Conference on Computer Vision and Pattern Recognition, pp. 4706–4715 (2020)
- [52] Jeong, J., Choi, J., Jo, D.U., Choi, J.Y.: Congestion-aware bayesian loss for crowd counting. *IEEE Access* **10**, 8462–8473 (2022)
- [53] Ma, Z., Wei, X., Hong, X., Gong, Y.: Bayesian loss for crowd count estimation with point supervision. In: Proceedings of the IEEE/CVF International Conference on Computer Vision, pp. 6142–6151 (2019)
- [54] Zhang, J., Cheng, Z.-Q., Wu, X., Li, W., Qiao, J.-J.: Crossnet: Boosting crowd counting with localization. In: Proceedings of the 30th ACM International Conference on Multimedia, pp. 6436–6444 (2022)
- [55] Lin, H., Ma, Z., Hong, X., Shangguan, Q., Meng, D.: Gramformer: Learning crowd counting via graph-modulated transformer. In: Proceedings of the AAAI Conference on Artificial Intelligence, vol. 38, pp. 3395–3403 (2024)
- [56] Meng, H., Hong, X., Lai, Z., Shang, M.: Free lunch enhancements for multi-modal crowd counting. In: Proceedings of the Computer Vision and Pattern Recognition Conference, pp. 14013–14023 (2025)
- [57] You, Z., Yang, K., Luo, W., Lu, X., Cui, L., Le, X.: Few-shot object counting with similarity-aware feature enhancement. In: Proceedings of the IEEE/CVF Winter Conference on Applications of Computer Vision, pp. 6315–6324 (2023)
- [58] Peng, S., Yin, B., Xia, Y., Yang, Q., Wang, L.: Semi-supervised crowd counting based on patch crowds statistics. In: 2022 Asia Conference on Algorithms, Computing and Machine Learning (CACML), pp. 749–755 (2022). IEEE
- [59] Lei, Y., Liu, Y., Zhang, P., Liu, L.: Towards using count-level weak supervision for crowd counting. *Pattern Recognition* **109**, 107616 (2021)

- [60] Meng, Y., Zhang, H., Zhao, Y., Yang, X., Qian, X., Huang, X., Zheng, Y.: Spatial uncertainty-aware semi-supervised crowd counting. In: Proceedings of the IEEE/CVF International Conference on Computer Vision, pp. 15549–15559 (2021)
- [61] Chan, A.B., Liang, Z.-S.J., Vasconcelos, N.: Privacy preserving crowd monitoring: Counting people without people models or tracking. In: 2008 IEEE Conference on Computer Vision and Pattern Recognition, pp. 1–7 (2008). <https://doi.org/10.1109/CVPR.2008.4587569>
- [62] Idrees, H., Saleemi, I., Seibert, C., Shah, M.: Multi-source multi-scale counting in extremely dense crowd images. In: 2013 IEEE Conference on Computer Vision and Pattern Recognition, pp. 2547–2554 (2013). <https://doi.org/10.1109/CVPR.2013.329>
- [63] Idrees, H., Tayyab, M., Athrey, K., Zhang, D., Al-Maadeed, S., Rajpoot, N., Shah, M.: Composition loss for counting, density map estimation and localization in dense crowds. In: Proceedings of the European Conference on Computer Vision (ECCV), pp. 532–546 (2018)
- [64] Chen, K., Loy, C.C., Gong, S., Xiang, T.: Feature mining for localised crowd counting. In: *Bmvc*, vol. 1, p. 3 (2012)
- [65] Zhang, C., Li, H., Wang, X., Yang, X.: Cross-scene crowd counting via deep convolutional neural networks. In: Proceedings of the IEEE Conference on Computer Vision and Pattern Recognition, pp. 833–841 (2015)
- [66] Wang, Q., Gao, J., Lin, W., Li, X.: Nwpu-crowd: A large-scale benchmark for crowd counting and localization. *IEEE transactions on pattern analysis and machine intelligence* **43**(6), 2141–2149 (2020)
- [67] Sindagi, V.A., Yasarla, R., Patel, V.M.: Jhu-crowd++: Large-scale crowd counting dataset and a benchmark method. *IEEE Transactions on Pattern Analysis and Machine Intelligence* **44**(5), 2594–2609 (2020)
- [68] Ristani, E., Solera, F., al.: Performance measures and a data set for multi-target, multi-camera tracking. In: *ECCV Workshop on Benchmarking Multi-Target Tracking* (2016)
- [69] Jaderberg, M., Simonyan, K., Zisserman, A., Kavukcuoglu, K.: Spatial transformer networks. In: *Advances in Neural Information Processing Systems*, pp. 2017–2025 (2015)
- [70] Wan, J., Liu, Z., Chan, A.B.: A generalized loss function for crowd counting and localization. In: Proceedings of the IEEE/CVF Conference on Computer Vision and Pattern Recognition (CVPR), pp. 1974–1983 (2021)

- [71] Xu, Y., Liu, X., Liu, Y., Zhu, S.C.: Multi-view people tracking via hierarchical trajectory composition. In: CVPR, pp. 4256–4265 (2016)
- [72] Fleuret, F., Berclaz, J., Lengagne, R., Fua, P.: Multicamera people tracking with a probabilistic occupancy map. *IEEE transactions on pattern analysis and machine intelligence* **30**(2), 267–282 (2007)
- [73] Teepe, T., Wolters, P., Gilg, J., Herzog, F., Rigoll, G.: Earlybird: Early-fusion for multi-view tracking in the bird’s eye view. In: Proceedings of the IEEE/CVF Winter Conference on Applications of Computer Vision (WACV) Workshops, pp. 102–111 (2024)
- [74] Alturki, R., Hilton, A., Guillemaut, J.-Y.: Enhanced multi-view pedestrian detection using probabilistic occupancy volume. In: Proceedings of the IEEE/CVF Conference on Computer Vision and Pattern Recognition (CVPR) Workshops, pp. 3386–3395 (2025)
- [75] Zhang, Q., Chan, A.B.: Wide-area crowd counting: Multi-view fusion networks for counting in large scenes. *International Journal of Computer Vision* **130**, 1938–1960 (2020)
- [76] He, K., Zhang, X., Ren, S., Sun, J.: Deep residual learning for image recognition. In: Proceedings of the IEEE Conference on Computer Vision and Pattern Recognition, pp. 770–778 (2016)
- [77] Liu, Z., Hu, H., Lin, Y., Yao, Z., Xie, Z., Wei, Y., Ning, J., Cao, Y., Zhang, Z., Dong, L., *et al.*: Swin transformer v2: Scaling up capacity and resolution. In: Proceedings of the IEEE/CVF Conference on Computer Vision and Pattern Recognition, pp. 12009–12019 (2022)
- [78] Ganin, Y., Ustinova, E., Ajakan, H., Germain, P., Larochelle, H., Laviolette, F., March, M., Lempitsky, V.: Domain-adversarial training of neural networks. *Journal of machine learning research* **17**(59), 1–35 (2016)
- [79] Wan, J., Chan, A.B.: Modeling noisy annotations for crowd counting. In: Neural Information Processing Systems (2020)
- [80] Liang, D., Xu, W., Bai, X.: An end-to-end transformer model for crowd localization. *European Conference on Computer Vision* (2022)
- [81] Han, T., Bai, L., Liu, L., Ouyang, W.: Steerer: Resolving scale variations for counting and localization via selective inheritance learning (2023)
- [82] Zhang, Y., Zhou, D., Chen, S., Gao, S., Ma, Y.: Single-image crowd counting via multi-column convolutional neural network. In: Proceedings of the IEEE/CVF Conference on Computer Vision and Pattern Recognition (CVPR), pp. 589–597 (2016)

- [83] Cheng, Z.-Q., Dai, Q., Li, H., Song, J., Wu, X., Hauptmann, A.G.: Rethinking spatial invariance of convolutional networks for object counting. In: Proceedings of the IEEE/CVF Conference on Computer Vision and Pattern Recognition, pp. 19638–19648 (2022)
- [84] Liu, C., Lu, H., Cao, Z., Liu, T.: Point-query quadtree for crowd counting, localization, and more. In: Proceedings of the IEEE/CVF International Conference on Computer Vision, pp. 1676–1685 (2023)
- [85] Chen, I.-H., Chen, W.-T., Liu, Y.-W., Yang, M.-H., Kuo, S.-Y.: Improving point-based crowd counting and localization based on auxiliary point guidance. In: European Conference on Computer Vision, pp. 428–444 (2024). Springer
- [86] Zhang, Q., Li, Y., Liu, Y., Zhou, Y., Jiao, J.: Diffusionloc: A diffusion model-based framework for crowd localization. *Image and Vision Computing* **155**, 105439 (2025)
- [87] Zhang, C., Li, H., Wang, X., Yang, X.: Cross-scene crowd counting via deep convolutional neural networks. In: 2015 IEEE Conference on Computer Vision and Pattern Recognition (CVPR), pp. 833–841 (2015). <https://doi.org/10.1109/CVPR.2015.7298684>
- [88] Liu, J., Gao, C., Meng, D., Hauptmann, A.G.: Decidenet: Counting varying density crowds through attention guided detection and density estimation. In: 2018 IEEE/CVF Conference on Computer Vision and Pattern Recognition, pp. 5197–5206 (2018). <https://doi.org/10.1109/CVPR.2018.00545>
- [89] Sam, D.B., Sajjan, N.N., Babu, R.V., Srinivasan, M.: Divide and grow: Capturing huge diversity in crowd images with incrementally growing cnn. In: 2018 IEEE/CVF Conference on Computer Vision and Pattern Recognition, pp. 3618–3626 (2018). <https://doi.org/10.1109/CVPR.2018.00381>
- [90] Miao, Y., Han, J., Gao, Y., Zhang, B.: St-cnn: Spatial-temporal convolutional neural network for crowd counting in videos. *Pattern Recognition Letters* **125**, 113–118 (2019)
- [91] Hafeezallah, A., Al-Dhamari, A., Abu-Bakar, S.A.R.: U-asd net: Supervised crowd counting based on semantic segmentation and adaptive scenario discovery. *IEEE Access* **9**, 127444–127459 (2021) <https://doi.org/10.1109/ACCESS.2021.3112174>
- [92] Cai, Y., Ma, Z., Lu, C., Wang, C., He, G.: Global representation guided adaptive fusion network for stable video crowd counting. *IEEE Transactions on Multimedia* **25**, 5222–5233 (2023) <https://doi.org/10.1109/TMM.2022.3189246>
- [93] Zhao, Z., Ma, P., Jia, M., Wang, X., Hei, X.: A dilated convolutional neural network for cross-layers of contextual information for congested crowd counting. *Sensors* **24**(6), 1816 (2024)